Modulation transfer function testing of detector arrays using narrow-band laser speckle

Martin Sensiper, MEMBER SPIE
Glenn D. Boreman, MEMBER SPIE
Alfred D. Ducharme
University of Central Florida
Center for Research in Electro-Optics and Lasers
Department of Electrical Engineering
Orlando, Florida 32816

Donald R. Snyder, MEMBER SPIE
U.S. Air Force Wright Laboratory
WL/MNGI
Eglin Air Force Base, Florida 32542

Abstract. A method for measuring the modulation transfer function (MTF) of a detector array from zero spatial frequency to twice the Nyquist frequency is presented. Laser speckle with a tunable, narrow spatial-frequency bandpass is used. The MTF measured with this method is compared to the MTF measured using sine targets. The results of the two methods agree to within 2%.

Subject terms: modulation transfer functions; laser speckle; detector arrays; charge-coupled devices; aliasing.

Optical Engineering 32(2), 395–400 (February 1993).

1 Introduction

Modulation transfer function (MTF) describes the spatial-frequency response of an image-forming system. Widespread use of staring focal-plane arrays (FPAs) has motivated a variety of instrumentation approaches for measuring their MTFs. To date, most techniques for measuring the MTFs of FPAs have involved imaging bar targets, sinusoidal targets, or knife edges.[1–3] These deterministic methods were originally used for measuring the MTFs of continuous-imaging systems. When FPAs that have discrete elements sample the images of such targets, the output depends on the phase of the target image with respect to the structure of the sampling array.[4–6] The extended knife-edge test[3,7] has been suggested as an approach to this phasing problem. A superresolution scan can be created if the knife edge is precisely oriented in angle with respect to the pixel columns. One disadvantage of these approaches is that the use of any small target, such as a knife edge, line source, or point source, will characterize the MTF based on the response of a limited region of the sensor rather than the entire array. In addition, the use of any imaged target for FPA testing is complicated by the fact that the MTF of the imaging optics must be considered.

Previous work[8,9] has demonstrated the feasibility of using laser speckle for MTF characterization of FPAs. The main advantages of this approach are that the entire array is tested, there is no lens required for target projection, and that the speckle is randomly positioned with respect to the FPA structure. The work in Refs. 8 and 9 used laser speckle patterns with a wide spatial-frequency content. This restricted the method to spatial frequencies below the Nyquist frequency, to avoid aliasing. In this paper, we generate speckle that is tunable and narrow band. This allows the MTFs of FPAs to be measured out to twice the Nyquist frequency.

Paper 21111 received Nov. 29, 1991; revised manuscript received June 6, 1992; accepted for publication June 6, 1992.
© 1993 Society of Photo-Optical Instrumentation Engineers. 0091-3286/93/$2.00.

Any method for measuring FPA MTF by targets larger than one pixel requires that the response of the detectors be corrected for gain and offset variations. The residual variation of detector response produces a baseline noise[10] that ultimately limits the precision of the measurement.

2 Instrument Design

Figure 1 shows the layout of the instrument. Laser radiation is diffusely reflected from the interior surfaces of the integrating sphere. Radiation reaching the output port of the sphere is of uniform irradiance[9] and has a phase that is uniformly distributed between 0 and 2π. The radiation passes through the aperture, which determines the spatial-frequency content of the speckle pattern that falls on the FPA. The coherent radiation that illuminates the aperture is of uniform irradiance, monochromatic, and of spatially random phase. The polarizer that follows the aperture makes the resulting laser speckle linearly polarized. These conditions ensure that the spatial-frequency power spectral density (PSD) of the speckle irradiance on the FPA is proportional to the autocorrelation of the aperture transmission function, plus a delta function at zero frequency.[11,12] The MTF of the FPA can be calculated, because we know the PSD of the input speckle pattern, and an accurate estimate of the output PSD can be made from the FPA response. The relationship among the PSDs and the MTF is

$$\mathrm{PSD}_{\mathrm{out}}(\xi,\eta) = [\mathrm{MTF}(\xi,\eta)]^2\ \mathrm{PSD}_{\mathrm{in}}(\xi,\eta)\ , \qquad (1)$$

where ξ and η are the spatial frequencies in the x and y directions. We are often concerned with measuring one profile of the MTF at a time. Assuming that $\mathrm{PSD}_{\mathrm{in}}$ is a separable function, Eq. (1) can then be written with only a ξ dependence, and $\mathrm{PSD}_{\mathrm{in}}(\xi)$ is then attenuated by $\mathrm{MTF}(\xi)$.

In Ref. 8, a square aperture was used, which produced a $\mathrm{PSD}_{\mathrm{in}}$ with a triangular shape. To avoid aliasing, the cutoff frequency of $\mathrm{PSD}_{\mathrm{in}}$ was set to the spatial Nyquist frequency of the FPA, which for detectors with a center-to-center spacing Δx is $\xi_{\mathrm{Ny}} = 1/(2\Delta x)$. Because $\mathrm{PSD}_{\mathrm{in}}$ decreased linearly from dc to ξ_{Ny}, the presence of white noise in the FPA

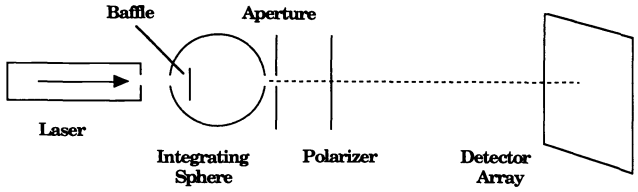

Fig. 1 Schematic of the test instrument.

response dictated that the signal-to-noise ratio in PSD_{out} was a decreasing function of frequency, and became insufficient at frequencies approaching ξ_{Ny}. The MTF measurement in Ref. 8 was thus limited to spatial frequencies somewhat below ξ_{Ny}. The instrument described in Ref. 9 used a similar square aperture but used an integrating sphere for generating the laser speckle.

The current configuration uses an integrating sphere with a double-slit aperture, which generates laser speckle with a PSD_{in} that is narrow band, tunable, and of constant magnitude. Ambiguities usually caused by aliasing are avoided by the use of a narrow-band input. A tunable, constant-magnitude input also facilitates high-frequency MTF measurements, because the input signal strength is not a decreasing function of ξ.

In the visible spectrum, we used a Spectra-Physics 165 argon laser with an intracavity etalon as the radiation source. The wavelength was 514 nm, with an output power of 200 mW. In the near infrared, we used a Spectra-Diode Labs SDL-5410-H1 laser diode at 848 nm with an output power of 100 mW. This laser has a linewidth of approximately 0.024 nm. The data shown in this paper are those taken using the argon laser, however the data taken using the near-infrared laser are comparable. A 25.4-mm-diam integrating sphere, with a diffuse white surface, was used for both wavelengths.

When ξ_{Ny}, the laser wavelength λ, and the dimensions of the output port of the integrating sphere are known, the aperture dimensions can be specified. The maximum aperture dimensions are determined by the size of the output port of the integrating sphere, under the requirement of uniform aperture illumination. The spatial frequency of any particular feature in the power spectrum scales as follows[11]:

$$\xi = \frac{x}{\lambda z} \ , \tag{2}$$

where x is the corresponding aperture dimension and z is the distance from the aperture to the observation plane.

An Electrim 1000 CCD camera was used in these experiments. The pixel spacing in the horizontal direction is 13.75 μm, which gives a Nyquist frequency of 36.36 c/mm. The detector array in this camera is 192 (horizontal) by 165 (vertical). Commercial CCD cameras designed for video applications often contain an antialiasing filter in the electronics, which attenuates the MTF at frequencies approaching ξ_{Ny}. The Electrim camera electronics did not contain such a filter, and thus was particularly well suited for demonstration of MTF measurements at frequencies past ξ_{Ny}.

2.1 *Narrow-Band Aperture*

Let $P(x,y)$ be the transmission function of the aperture.

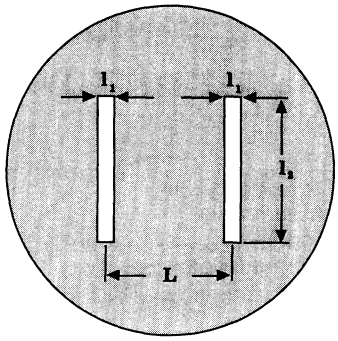

Fig. 2 Narrow-band aperture: $L = 1.651$ mm, $l_1 = 0.127$ mm, and $l_2 = 2.032$ mm.

Referring to Fig. 2, this can be written as

$$P(x,y) = \mathrm{rect}\left(\frac{x}{l_1}, \frac{y}{l_2}\right) * [\delta(x + L/2) + \delta(x - L/2)] \ , \tag{3}$$

where $*$ is the convolution operator, l_1 and l_2 are slit dimensions, and L is the slit spacing. Using the method of Refs. 11 and 12, the PSD_{in} of the irradiance of the speckle at the FPA can be written as a delta function at dc added to the normalized autocorrelation of $P(x,y)$. The function in Eq. (3) is separable in x and y. The one-dimensional $PSD_{in}(\xi)$ is the $\eta = 0$ profile of $PSD_{in}(\xi,\eta)$. The one-dimensional input PSD can be written as

$$\mathrm{PSD}_{in}(\xi) = \langle I \rangle^2 \left[\begin{array}{l} \delta(\xi) + \frac{1}{2} \frac{(\lambda z)^2}{l_1 l_2} \mathrm{tri}\left(\frac{\xi}{l_1/\lambda z}\right) \\ + \frac{1}{4} \frac{(\lambda z)^2}{l_1 l_2} \mathrm{tri}\left(\frac{\xi - L/\lambda z}{l_1/\lambda z}\right) \\ + \frac{1}{4} \frac{(\lambda z)^2}{l_1 l_2} \mathrm{tri}\left(\frac{\xi + L/\lambda z}{l_1/\lambda z}\right) \end{array} \right] \ . \tag{4}$$

In Eq. (4), $\mathrm{tri}(x) = 1 - |x|$ for $|x| \leq 1$ and zero elsewhere, and $\langle I \rangle^2$ is the square of the average speckle irradiance. Figure 3 shows this one-dimensional input PSD along the ξ direction, consisting of a baseband triangle centered at dc and sideband triangles centered at the carrier frequencies, $\xi = \pm L/(\lambda z)$. The features in the power spectrum scale with z, as indicated by Eq. (2). As the FPA is moved toward the aperture and z is decreased, the sideband triangles move toward higher frequencies and the base of all the triangles expand. At aperture-to-FPA distances in which the sideband triangles are located above ξ_{Ny} the triangles are aliased symmetrically about ξ_{Ny} into lower frequencies. Because the location and the limits of the spatial frequencies in the speckle are known, there is no ambiguity about whether or not any particular data set is aliased. The high-frequency limit of the test is set, as z is decreased, by the point at which the sideband triangles, aliased into lower and lower frequencies, begin to overlap the baseband triangle. This occurs just before $2\xi_{Ny}$. The method by which the MTF is calculated from the raw data is described in Sec. 3.

2.2 *Extended-Frequency Aperture*

The concept of driving an optical system with a wideband

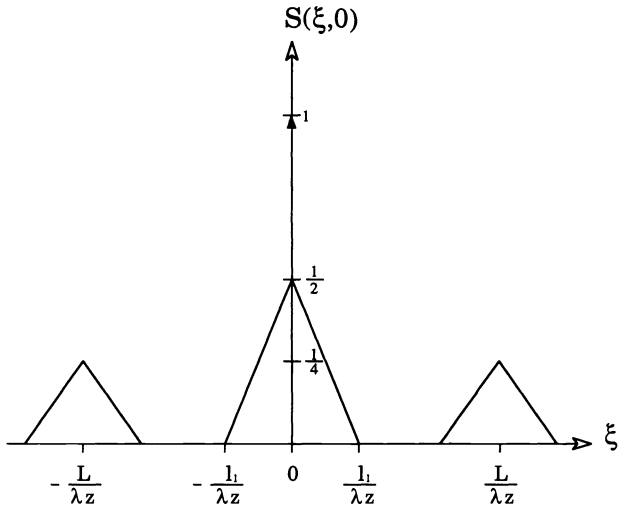

Fig. 3 $PSD_{in}(\xi)$ resulting from the narrow-band aperture.

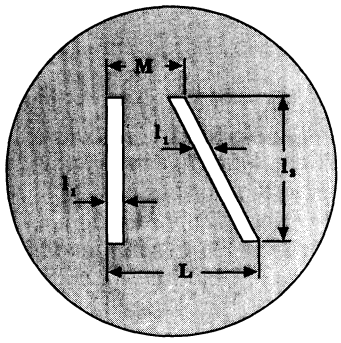

Fig. 4 Extended-frequency aperture: $L = 1.651$ mm, $M = 0.762$ mm, $l_1 = 0.127$ mm, and $l_2 = 2.032$ mm.

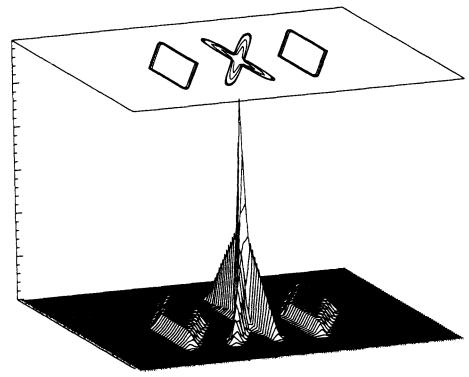

Fig. 5 $PSD_{in}(\xi,\eta)$ resulting from the extended-frequency aperture.

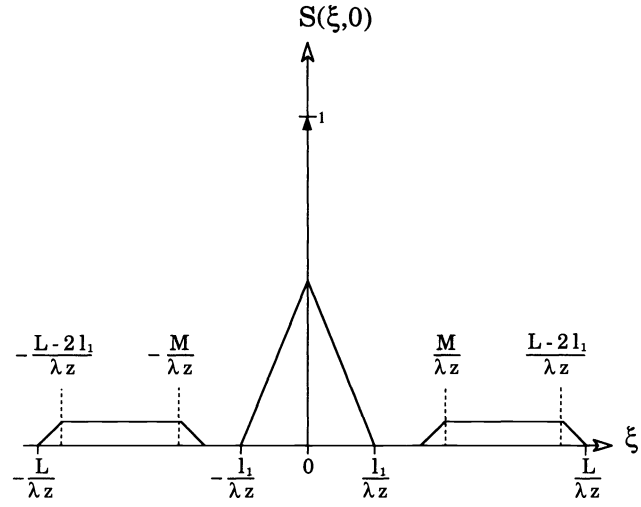

Fig. 6 $PSD_{in}(\xi)$ resulting from the extended-frequency aperture.

random input, as a method for finding the system response, was initially limited by the lack of a random chart whose spatial-frequency content was constant over a sufficiently wide bandwidth.[13] When used in the instrument shown in Fig. 1, the aperture shown in Fig. 4 generates laser speckle with a constant frequency content over an appreciable range of frequencies. This aperture is not separable in x and y. A numerical calculation of the two-dimensional PSD of the resulting speckle is shown in Fig. 5. A one-dimensional profile of the PSD is shown in Fig. 6. The frequency limits of PSD_{in} are related through Eq. (2) to the geometry of the aperture. PSD_{in} is constant for $M/\lambda z < \xi < (L - 2l_1)/\lambda z$, where M and L are the minimum and maximum slit spacings.

3 Data Processing

3.1 *Narrow-Band Aperture*

A representative sample of the speckle detected by the array, using the aperture in Fig. 2, is shown in Fig. 7. The data exhibit both random phase and narrow spatial-frequency content. Speckle data were collected at 60 aperture-to-FPA distances ranging from 45 to 2120 mm. Each horizontal row of data is a single observation of an ergodic random process. The magnitude squared of the one-dimensional discrete Fourier transform (DFT) of each row gives a single estimate of the one-dimensional power spectrum, $PSD_{out}(\xi)$. These spectra are ensemble averaged over the number of rows of detectors in the FPA to reduce the noise inherent in PSD estimates from finite-length data sets, and thus produce a more accurate estimate of $PSD_{out}(\xi)$.

Figure 3 and Eq. (4) illustrate that the baseband triangle centered at zero frequency has twice the amplitude of the sideband triangles. The height of the sideband triangles is attenuated by the FPA MTF at the frequency where they are located. The baseband triangle peak can be normalized to 1. We can determine the amount of attenuation caused by the FPA MTF by comparing the (unattenuated) peak height of the baseband triangle with the peak height of a sideband triangle. However, the value at the peak of the baseband triangle is masked by the delta function at dc, as seen in Eq. (4).

We excise the delta function by inverse Fourier transforming the average power spectrum $PSD_{out}(\xi)$ to obtain an average autocorrelation $R(x)$. In this domain, the zero-frequency delta function in the PSD is now a constant offset and is the minimum value of $R(x)$. We subtract this minimum value and retransform to yield $PSD_{out}(\xi)$ with the delta function at dc excised. This leaves the dc value of the

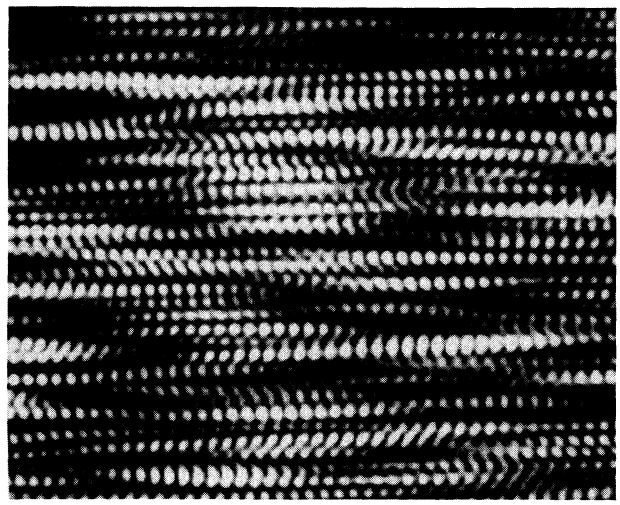

Fig. 7 Representative speckle pattern obtained with the narrow-band aperture.

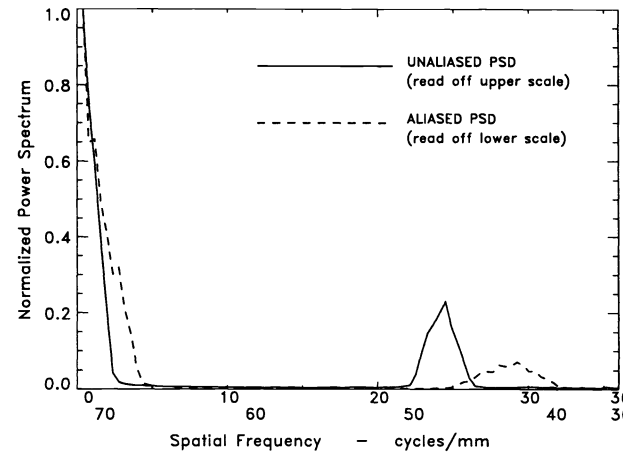

Fig. 8 Examples of $PSD_{out}(\xi)$ for the narrow-band aperture, both above and below ξ_{Ny}.

baseband triangle intact and allows the MTF to be correctly normalized to 1 at $\xi = 0$.

When a DFT is performed on a data set of length N, the Nyquist frequency appears at the $N/2$ component of the DFT output. A ratio can be formed to evaluate the spatial frequency ξ_n that corresponds to the n'th component as

$$\frac{\xi_{Ny}}{N/2} = \frac{\xi_n}{n} \quad . \tag{5}$$

This associates frequencies between zero and ξ_{Ny} with DFT components from 0 to the $N/2$ component. Spatial frequencies present in PSD_{in}, but between ξ_{Ny} and $2\xi_{Ny}$, are aliased symmetrically about the Nyquist frequency into the frequency band extending from ξ_{Ny} back to zero. Unambiguous determination of whether the values found for the transform components pertain to aliased or unaliased frequencies is possible because of the narrow-band nature of $PSD_{out}(\xi)$. We can unfold the aliased frequencies and plot PSD_{out} from zero to $2\xi_{Ny}$.

We plot two representative (positive-frequency) profiles of $PSD_{out}(\xi)$ in Fig. 8, which are ensemble averages over the 165 rows of data contained in a single frame. The unaliased spatial frequencies (solid line) are noted along the horizontal axis from zero to ξ_{Ny}, and the aliased frequencies (dotted line) are noted, below their low-frequency aliases, from ξ_{Ny} to $2\xi_{Ny}$. Because we know the spatial frequency of the input from Eq. (2) for each image, there is no doubt about whether or not the triangle is aliased. The data can be read off the appropriate scale and unfolded to form a curve from zero to ξ_{Ny}. Using Eq. (1), we can calculate one point at a time on the MTF curve. The MTF calculated from these data is shown in Sec. 4.

For frequencies within one triangle width of ξ_{Ny}, there is an overlap of triangles representing the aliased and unaliased components of the narrow-band input. This overlap increases the measured PSD_{out}. This can be seen in our measured MTF values just adjacent to ξ_{Ny}. When the input is at ξ_{Ny}, PSD_{out} increases by a factor of 2 because of this overlap, which has been divided out in our results. Points on the MTF curve at frequencies that are one triangle width removed from ξ_{Ny} are not affected by overlap. This effect is not a problem near dc, because for low frequencies, the width of the triangles has decreased enough to prevent overlap between the zeroth DFT component (dc) and the first DFT component.

During collection of the data, the approximate aperture-to-FPA distance was recorded. Displacements from the desired distance, or a slight tilt in the aperture-to-pixel column alignment can shift the triangle peak. The approximate distance and Eqs. (1) and (2) are used to search for the peak as a local maximum in the transform components. Because each component in the DFT can be associated with a specific spatial frequency, we can determine the spatial frequency at which the peak occurs, to within the resolution of the DFT. The procedure of frequency determination is essentially self-calibrating.

3.2 *Extended-Frequency Aperture*

The processing of the two-dimensional data can be done in a similar manner. Figure 9 shows a sample of the two-dimensional speckle data. Because the aperture (Fig. 4) is not separable in x and y, neither the speckle data nor the PSDs are separable in ξ and η. Two-dimensional DFTs of the data must be performed and the two-dimensional power spectra must be averaged. An example of PSD_{out} (ξ,η) is shown in Fig. 10 as a two-dimensional top view. This output spectrum is the response of the FPA to the PSD_{in} shown in Fig. 5. Figure 10 is an average of the two-dimensional spectra from 50 frames of speckle data.

The $PSD_{out}(\xi)$ is seen to be attenuated by MTF(ξ). The PSD_{in} is constant over a range of frequencies, so data about the squared MTF over that range are obtained directly from the shape of PSD_{out}. However, there is a penalty in the signal-to-noise ratio compared to the narrow-band case, because a given amount of laser power is now spread over a range of spatial frequencies, rather than being concentrated at a single frequency. A ξ profile of MTF could be calculated from these data, but more frame averaging would be needed to obtain useful results.

4 MTF Results

The MTF in the horizontal direction for the Electrim 1000

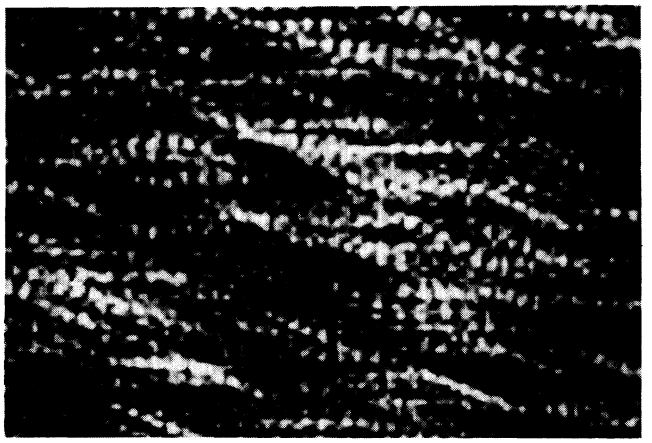

Fig. 9 Representative speckle pattern obtained with the extended-frequency aperture.

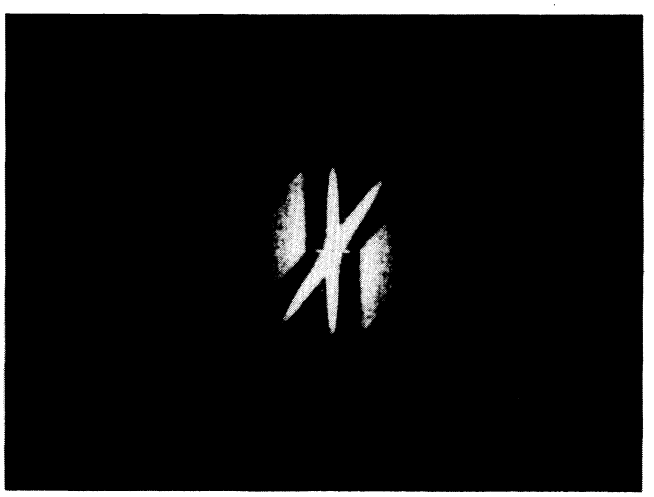

Fig. 10 $PSD_{out}(\xi,\eta)$ resulting from the extended-frequency aperture.

FPA is presented in Fig. 11 (solid line). The data points are shown along with a third-order polynomial fitted to the points. These measurements were made with the narrow-band aperture.

To compare our MTF results for the FPA with results from sine-wave testing (which requires the use of an imaging lens), we obtained the MTF for the imaging lens using an Ealing Eros MTF analyzer. The lens and the FPA were then used to measure the system response by imaging precision sinusoidal test targets from a commercial transparency.[14] The MTF at each frequency was calculated as

$$\mathrm{MTF}(\xi)=\frac{\mathrm{pixel}_{\max}-\mathrm{pixel}_{\min}}{\mathrm{pixel}_{\max}+\mathrm{pixel}_{\min}}\ , \tag{6}$$

where $\mathrm{pixel}_{\max}$ and $\mathrm{pixel}_{\min}$ are adjacent maximum and minimum values in the sine-wave data.

The product of the FPA MTF and the lens MTF should equal the system MTF measured by imaging the sinusoids. This comparison is seen in Fig. 11. The curves agree to within 2%. The narrow-band speckle MTF method measured the MTF of the FPA to 1.6 times ξ_{Ny}.

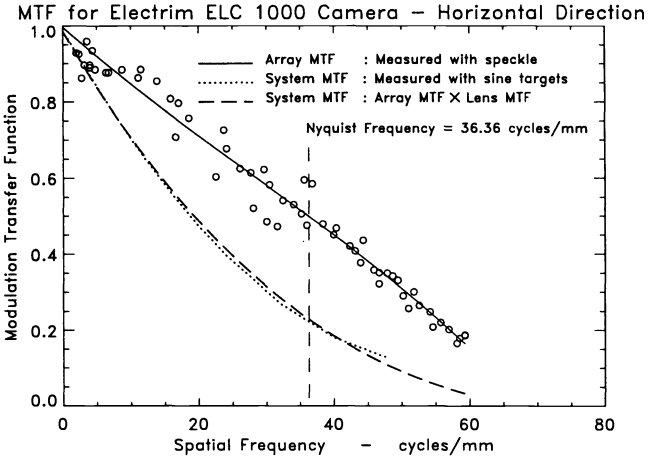

Fig. 11 MTF results: solid line is FPA MTF measured with narrow-band laser speckle; dashed line is the product of FPA MTF (solid line) and MTF of the lens alone; and dotted line is the combined MTF of the FPA and lens, measured with sine targets.

5 Conclusions

We have demonstrated the use of laser speckle for measuring the MTF of detector arrays from dc to 1.6 times ξ_{Ny}. Our results are within 2% of those from a standard sine-wave measurement. The method is essentially self-calibrating in that the spatial frequency for any data point is a measured value. Because the optical path contains no imaging optics, the method measures the MTF of the FPA directly. This method produces a test target that is randomly phased with respect to the FPA structure and is applicable over a wide range of wavelengths.

Acknowledgments

This work was supported by the U.S. Air Force, Wright Laboratory, under contract DAA-B07-88-C-F-405-ARPA-6324.

References

1. S. B. Campana, "Techniques for evaluating charge coupled imagers," *Opt. Eng.* **16,** 2267–2274 (1977).
2. S. K. Park, R. Schowengerdt, and M. Kaczynski, "Modulation-transfer-function analysis for sampled image systems," *Appl. Opt.* **23,** 2572–2582 (1984).
3. S. E. Reichenbach, S. K. Park, and R. Narayanswamy, "Characterizing digital image acquisition devices," *Opt. Eng.* **30,** 170–177 (1991).
4. W. Wittenstein, J. C. Fontanella, A. R. Newbery, and J. Baars, "The definition of the OTF and the measurement of aliasing for sampled imaging systems," *Opt. Acta* **29,** 41–50 (1982).
5. R. Legault, "The aliasing problems in two-dimensional sampled imagery," in *Perception of Displayed Information,* L. M. Biberman, Ed., pp. 279–312, Plenum, New York (1973).
6. J. Feltz and M. Karim, "Modulation transfer function of charge-coupled devices," *Appl. Opt.* **29,** 717–722 (1990).
7. H. Wong, "Effect of knife-edge skew on modulation transfer function measurements of charge-coupled device imagers employing a scanning knife edge," *Opt. Eng.* **30,** 1394–1398 (1991).
8. G. Boreman and E. Dereniak, "Method for measuring modulation transfer function of charged-coupled devices using laser speckle," *Opt. Eng.* **24,** 148–150 (1986).
9. G. Boreman, Y. Sun, and A. James, "Generation of laser speckle with an integrating sphere," *Opt. Eng.* **29,** 339–342 (1990).
10. G. Boreman and C. Costanzo, "Compensation for gain nonuniformity and nonlinearity in HgCdTe infrared CCD focal planes," *Opt. Eng.* **26,** 981–984 (1987).
11. J. Goodman, "Statistical properties of laser speckle patterns," in *Laser Speckle and Related Phenomena,* J. C. Dainty, Ed., pp. 35–40, Springer-Verlag, Berlin (1975).

12. L. Goldfischer, "Autocorrelation function and power spectral density of laser-produced speckle patterns," *J. Opt. Soc. Am.* **55,** 247–253 (1965).
13. H. Kubota and H. Ohzu, "Method of measurement of response function by means of random chart," *J. Opt. Soc. Am.* **47,** 666–667 (1957).
14. Sine Patterns Catalog, Sine Patterns Inc., Penfield, NY (1990).

Martin Sensiper received his BS and MS degrees in electrical engineering from the University of Central Florida in 1989 and 1991, respectively. He was a graduate research assistant in the Infrared Systems Laboratory at the University of Central Florida/CREOL. He is currently employed at Martin Marietta in Orlando, Florida, where he is involved with testing quantum well focal plane arrays.

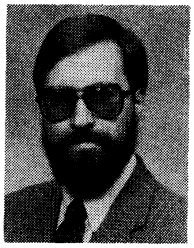

Glenn D. Boreman is an associate professor of electrical engineering in the Center for Research in Electro-Optics and Lasers (CREOL) at the University of Central Florida. He received a BS from the Institute of Optics, University of Rochester, and a PhD from the Optical Sciences Center, University of Arizona. He has held visiting research positions at IT&T, Texas Instruments, U.S. Army Night Vision Lab, and McDonnell Douglas. Dr. Boreman serves as topical editor for *Applied Optics* in the areas of radiometry and detectors and is past-president of the Florida Optical Society.

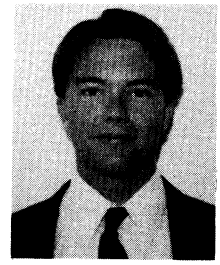

Alfred D. Ducharme received the BSEE degree from the University of Lowell, now known as the University of Massachusetts at Lowell, in 1990 and the MSEE degree from the University of Central Florida in 1992. He is now pursuing his PhD degree in electrical engineering while working as a graduate research assistant at the Center for Research in Electro-Optics and Lasers. His research interests include statistical optics and laser speckle.

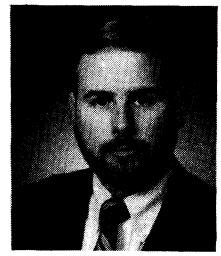

Donald R. Snyder is chief engineer of the Instrumentation Technology Branch, Advanced Guidance Division of the Air Force Wright Laboratory at Eglin Air Force Base, Florida. Mr. Snyder received a BS in physical electronics from the University of West Florida and is currently enrolled in graduate studies at the University of Florida Graduate Engineering and Research Center at Fort Walton Beach, Florida. He previously worked for the Air Force and Army in developing EO and missile test systems and with Honeywell in Clearwater, Florida in the areas of active and passive infrared remote sensing. He is a member of SPIE, OSA, and AOC and has authored 30 technical publications. Mr. Snyder has served SPIE as chairman of the High Speed Working Group and as the High Speed Conference co-chair for 1991. His research activities include high-speed imaging systems, high-definition video sensors, fiber optic remote sensing, and laser radar.